Goos-Hänchen shift and localization of optical modes in deformed microcavities

Julia Unterhinninghofen and Jan Wiersig
Institut für Theoretische Physik, Universität Bremen, Postfach 330 440, D-28334 Bremen, Germany

Martina Hentschel
Max-Planck-Institut für Physik komplexer Systeme, Nöthnitzer Straße 38, D-01187 Dresden, Germany

(Received 5 March 2008; published 1 July 2008)

Recently, an interesting phenomenon of spatial localization of optical modes along periodic ray trajectories near avoided resonance crossings has been observed [Wiersig, Phys. Rev. Lett. **97**, 253901 (2006)]. For the case of a microdisk cavity with elliptical cross section, we use the Husimi function to analyze this localization in phase space. Moreover, we present a semiclassical explanation of this phenomenon in terms of the Goos-Hänchen shift, which works very well even deep in the wave regime. This semiclassical correction to the ray dynamics modifies the phase-space structure such that modes can localize either on stable islands or along unstable periodic ray trajectories.

DOI: 10.1103/PhysRevE.78.016201 PACS number(s): 05.45.Mt, 42.25.−p

I. INTRODUCTION

The phenomenon of avoided level crossings was discovered more than 70 years ago by von Neumann and Wigner [1]. Two energy levels undergo an avoided crossing under variation of a control parameter when they first approach very close to one another, and then depart from each other without crossing. The energies E_j of eigenstates in closed quantum-mechanical systems are real valued. In open systems, the energy eigenstates are replaced by quasibound or resonant states with complex energies E_j [2,3]. The imaginary part determines the lifetime $\tau_j \propto 1/\mathrm{Im}(E_j)$ of the decaying state. The corresponding generalizations of avoided level crossings are avoided *resonance* crossings (ARCs) [4]. ARCs have been studied in a number of physical settings, such as laser-assisted electron-atom scattering [5], predissociation dynamics of molecules [6], biased multiple quantum wells [7], coupled quantum dots [8], quantum-dot microcavity systems [9–11], microwave cavities [12,13], and optical microcavities [14,15]. In the latter systems the electromagnetic modes and their frequencies play the role of eigenstates and their energies. One interesting phenomenon that can occur near ARCs is the formation of fast- and slowly decaying states [12,16].

In a recent letter it has been shown that this formation of fast and slowly decaying states can be accompanied by a localization of the states along unstable (or marginally unstable) periodic trajectories of the underlying classical system [15]. This localization is somewhat similar to the well-known effect of scarring, originally discovered for closed chaotic systems in the field of quantum chaos [17,18].

The aim of the present paper is twofold. First, we discuss the change of the *phase-space structure* of modes in optical microcavities when such localization near an ARC occurs. The phase-space picture allows clear identification of the physical mechanism of lifetime enhancement (reduction): destructive (constructive) interference in real space leads to a reduction (enhancement) of intensity in the leaky region of phase space. Second, we present a semiclassical explanation of the appearance of localized modes near ARCs based on an augmented ray dynamics in which the Goos-Hänchen shift (GHS) is included. The GHS is a lateral shift of totally reflected beams along the optical interface [19], i.e., the points of incidence and reflection do not coincide. Rather, the beam appears to travel, as an evanescent wave, a short distance through the optically thinner medium. The GHS is proportional to the wavelength λ. In the short-wavelength limit $\lambda \to 0$ the GHS therefore disappears, leading to the standard ray dynamics of geometric optics. In the field of quantum chaos, the short-wavelength limit corresponds to the classical limit. For finite wavelength λ, the GHS can be regarded as a semiclassical correction to the ray dynamics.

The paper is organized as follows. The system is defined in Sec. II. Section III presents the numerical analysis of localization of modes near ARCs. The semiclassical description in terms of the GHS is explained in Sec. IV. Finally, a summary is given in Sec. V.

II. SYSTEM

As model system we choose an optical microdisk with elliptical cross section. Microdisks allow light to be confined by total internal reflection at the boundary, which is highly relevant for various research fields and applications [20]. Microdisks with deformed cross section have attracted considerable attention in the context of quantum chaos in open systems [21,22]. Elliptical microdisks have been studied both theoretically [23,24] and experimentally [25,26]. As semimajor axis we set $a=R(1+\varepsilon)$ and as semiminor axis $b=R/(1+\varepsilon)$. The area of the ellipse πab does not depend on the deformation parameter ε. The eccentricity is given by $e=\sqrt{1-(b/a)^2}=\sqrt{1-1/(1+\varepsilon)^4}$. We choose $R=1$ μm and the effective index of refraction $n=3.3$ according to recent experiments on circular microdisks [11]. Maxwell's equations for the transverse magnetic (TM) polarized modes $E_z(x,y,t)=\psi(x,y)e^{-i\omega t}$ reduce to a two-dimensional scalar wave equation [27]

$$-\nabla^2\psi = n^2(x,y)\frac{\omega^2}{c^2}\psi, \tag{1}$$

with frequency ω and the speed of light in vacuum c. The wave function ψ and its normal derivative are continuous

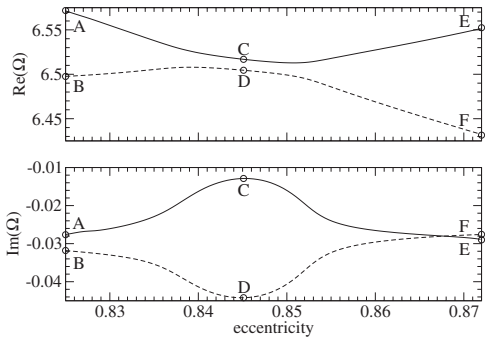

FIG. 1. An avoided resonance crossing in the elliptical microcavity. Plotted are the complex frequencies Ω as a function of the eccentricity. The real part shows an avoided crossing, whereas the imaginary part shows the formation of a long-lived mode C and a short-lived mode D. Dots mark the frequency of the modes shown in Fig. 2.

across the boundary of the cavity. At infinity, outgoing wave conditions are imposed. With these open boundary conditions the modes decay, as light can leak out of the cavity. This results in quasibound states with complex frequencies ω in the lower half plane. The real part is the usual frequency. The imaginary part is related to the lifetime $\tau=-1/[2\ \mathrm{Im}(\omega)]$ and to the quality factor $Q=-\mathrm{Re}(\omega)/[2\ \mathrm{Im}(\omega)]$.

III. AVOIDED RESONANCE CROSSINGS

We compute the modes numerically using the boundary element method [28]. Figure 1 shows the calculated normalized frequency $\Omega=\omega R/c=kR$ as a function of the eccentricity e. The considered region around $\mathrm{Re}(\Omega)=6.5$ corresponds to a vacuum wavelength of about 970 nm. We observe that the real part of the frequency performs an avoided crossing, and the imaginary part shows formation of a short-lived [large $|\mathrm{Im}(\Omega)|$] and a long-lived state [small $|\mathrm{Im}(\Omega)|$]. This is an ARC of external coupling in the strong-coupling regime [15]. Observing an avoided crossing is the more remarkable when we recall that the corresponding closed system with vanishing wave intensity on the boundary—the so-called elliptical billiard [29,30]—belongs to the class of integrable systems which typically do not show avoided level crossings [31].

The corresponding spatial mode structures are depicted in Fig. 2. The modes A and B at the left-hand side of the ARC and the modes E and F at its right-hand side look very similar to the states in the elliptical billiard [29]. These states can be labeled by two mode numbers n_1 and n_2. With n_1 (n_2) we count the nodal lines in the radial (azimuthal) direction in an elliptical coordinate system [29]. Note that, strictly speaking, the wave function of a quasibound state does not possess nodal lines, only the real and the imaginary parts of the wave function do. For modes A and F we find $(n_1,n_2)=(2,26)$, and for modes B and E we find $(n_1,n_2)=(3,18)$.

The hybridized modes C and D, however, have no counterparts in the elliptical billiard. They are superpositions of the original modes A and B (or E and F) shown in Fig. 2. We

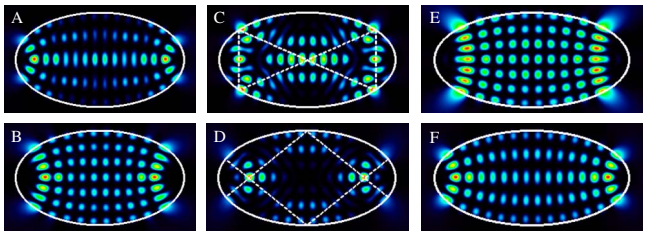

FIG. 2. (Color online) Calculated near-field intensity of modes with the same labels as in Fig. 1. The long-lived "bowtie" mode C and the short-lived mode D show localization along periodic ray trajectories (dashed lines).

can observe a clear accumulation of intensity on periodic ray trajectories. As these ray trajectories are marginally stable [29], such modes have been referred to as "scarlike" in Ref. [15]. True scars refer to the localization of modes along unstable periodic ray trajectories in chaotic systems [17]. It is customary to use the terminology "scars" also for systems with mixed phase space; see, e.g., Refs. [32–36]. Scarring has also been observed in microcavities [37–41].

What causes the lifetime enhancement of the bowtie-shaped mode C and the lifetime reduction of mode D? In Ref. [15], it was shown that the lifetime enhancement (reduction) of modes in rectangular cavities is due to destructive (constructive) interference at dielectric corners. Scattering at dielectric corners is the main decay channel in this kind of cavity. For the elliptical cavity there are no corners. To understand the lifetime modifications in this and other cavities without corners it is convenient to analyze the (emerging) Husimi function [42], representing the wave analog of the phase space. A phase-space representation of the ray dynamics is the so-called Poincaré surface of section (SOS), as shown in Fig. 3. Whenever the trajectory leaves the cavity's boundary after being reflected, its position s (arclength coordinate along the circumference) and tangential momentum $p=\sin\chi$ (the angle of incidence χ is measured from the surface normal) are recorded. It is a special property of integrable systems that each trajectory is confined to a

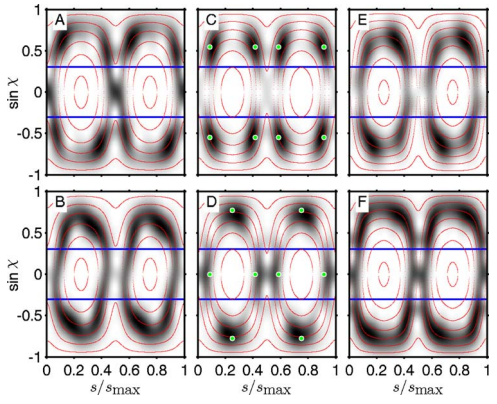

FIG. 3. (Color online) Emerging Husimi function (shaded regions) of the modes in Fig. 2. The horizontal lines are the critical lines $\sin\chi_c=\pm 1/n$. Dotted curves mark some invariant curves in the phase space of the ray dynamics. Thick dots represent the periodic ray trajectories on which the modes C and D are localized.

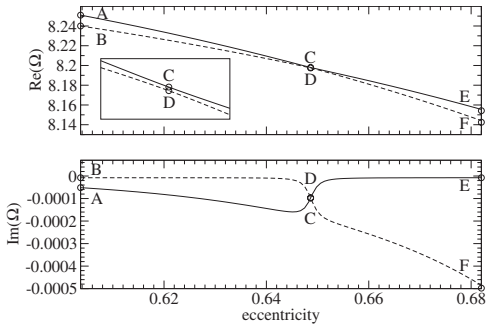

FIG. 4. An avoided resonance crossing with an avoided crossing in the real part of the frequency and a crossing in the imaginary part. Dots mark the frequency of the modes shown in Fig. 5. Inset shows a magnification of the avoided crossing.

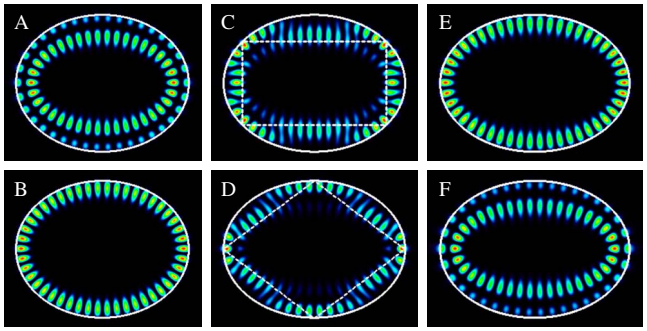

FIG. 5. (Color online) Calculated near-field intensity of the modes with the same labels as in Fig. 4. The rectangular-shaped mode *C* and the diamond-shaped mode *D* show localization along periodic ray trajectories (dashed lines).

so-called invariant curve (a torus in the full phase space). The invariant curve is exemplarily indicated by the dotted curves in Fig. 3. The symmetry properties of these curves in the SOS are determined by the discrete spatial symmetries of the billiard under investigation and the $p \rightarrow -p$ symmetry. The latter is due to time-reversal symmetry and hard-wall boundary conditions. The region between the two critical lines for total internal reflection $\sin \chi_c = \pm 1/n$ is called the leaky region. A ray that enters this region escapes according to Snell's and Fresnel's laws.

From Fig. 3 we can learn that, far away from the ARC, the modes *A*, *B*, *E*, and *F* follow roughly the ray dynamics as they are located near invariant curves. Note that the $p \rightarrow -p$ symmetry present in the corresponding billiard is broken in the open microcavity [43,44]. By comparing modes *A* and *B* with modes *C* and *D*, it is apparent that near the ARC a rearrangement of the phase-space structure takes place. The mode *D* has an enhanced intensity inside the leaky region leading to a reduction of its lifetime. The mode *C*, however, has strongly suppressed intensity in the leaky region of phase space, which increases its lifetime. Moreover, the phase-space picture shows clearly the localization of the modes along periodic ray trajectories (thick dots in Fig. 3).

In the following we demonstrate that the appearance of localized modes at ARCs is not necessarily associated with the formation of short- and long-lived modes. Figure 4 shows an example. Instead of the formation of a long- and a short-lived mode, we see a crossing in the imaginary parts, which is a signature of an ARC of internal type in the strong-coupling regime [14].

The corresponding mode patterns are depicted in Fig. 5. The unperturbed modes *A* and *B* (*E* and *F*) show a whispering-gallery structure similar to modes in a circular microdisk. The mode numbers are $(n_1, n_2) = (1, 38)$ for mode *A* and (0,46) for mode *B*. Also, this type of ARC leads to hybridized modes *C* and *D*, having strong localization along periodic ray trajectories.

The localization is also clearly visible in the phase-space representation in Fig. 6. Moreover, this representation explains why there is no formation of short- and long-lived states in this case. Mode *A* exists closer to the leaky region than mode *B*. Hence, the tail of mode *A* has a larger contribution inside the leaky region (even though the intensity is so weak that it cannot be seen in the figure). This explains why the lifetime of mode *A* is much shorter (by about a factor of 10) than the lifetime of mode *B*. Due to their very different contributions in the leaky region, a superposition of modes *A* and *B* cannot lead to a significant cancellation of phase-space intensity in the leaky region. Consequently, short- and long-lived modes cannot form.

The observed localization patterns can be explained for the cavities where the corresponding billiard is integrable. The hybridized modes, e.g., *C* and *D* in Fig. 5, are superpositions of the unperturbed modes far away from the ARC, e.g., *A* and *B* in Fig. 5. As the eigenstates of an integrable billiard, the unperturbed modes ψ have a simple structure of nodal lines. Therefore they can be labeled by a pair of mode numbers (n_1, n_2) and (m_1, m_2). The morphology of superpositions $\alpha\psi_{n_1,n_2} + \beta\psi_{m_1,m_2}$ is strongly influenced by the differences $|n_1 - m_1|$ and $|n_2 - m_2|$. If the differences are small numbers compared to n_i and m_i, then the mode pattern can be decomposed into a strongly oscillating part and a weakly varying envelope. The weakly varying envelope defines the localization pattern. Figure 7 illustrates this scenario for the simpler case of a rectangular billiard. The modes can be computed analytically:

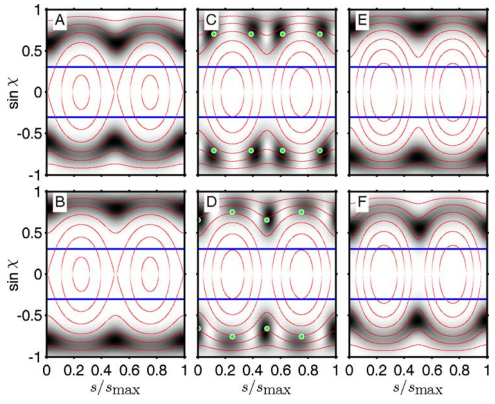

FIG. 6. (Color online) Emerging Husimi function (shaded regions) of modes in Fig. 5. The horizontal lines mark the critical lines $\sin \chi_c = \pm 1/n$. Dotted curves correspond to invariant curves in the phase space of the ray dynamics. Thick dots represent the periodic rays on which the modes *C* and *D* are localized.

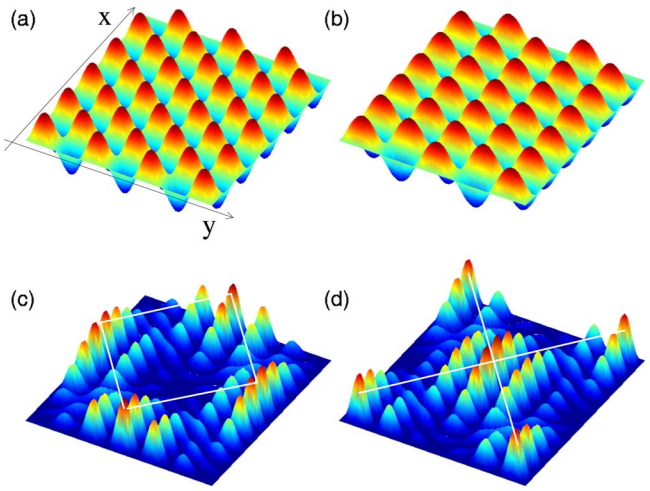

FIG. 7. (Color online) Eigenmodes and superpositions of eigenmodes in a rectangular billiard. (a) $\psi_{10,7}(x,y)$, (b) $\psi_{12,5}(x,y)$, (c) $|\psi_{10,7}-\psi_{12,5}|^2$, and (d) $|\psi_{10,7}+\psi_{12,5}|^2$. Lines mark periodic ray trajectories.

$$\psi_{n_x,n_y}(x,y) = \sin\left(\frac{\pi n_x}{R}x\right)\sin\left(\frac{\pi n_y}{\varepsilon R}y\right), \tag{2}$$

if $0 \le x \le R$ and $0 \le y \le \varepsilon R$; otherwise $\psi_{n_x,n_y}(x,y)=0$. The positive integers n_x and n_y count the number of nodal lines in the x and y directions (boundaries $x=0$ and $y=0$ are not counted), respectively. Figures 7(a) and 7(b) show the cases $(n_x,n_y)=(10,7)$ and $(m_x,m_y)=(12,5)$. It can be seen that the superposition $\psi_{10,7}-\psi_{12,5}$ has reduced intensity at the corner regions due to destructive interference. Correspondingly, the intensity near the center points is enhanced due to constructive interference. The opposite is true for the superposition $\psi_{10,7}+\psi_{12,5}$. In both cases the localization resembles scarring on periodic ray trajectories of short period.

IV. GOOS-HÄNCHEN SHIFT

In the previous section we demonstrated the existence of localized modes in optical microcavities near ARCs. But why is the light intensity in such a situation localized along periodic ray trajectories? To find an answer to this question we compare in Fig. 8 the incident and the emerging Husimi functions [42] for $p=0.75$. The incident (emerging) Husimi function represents the optical mode before (after) the reflection at the boundary of the microcavity. A lateral shift of about $\Delta s=0.011 s_{\max}$ can be observed. We interpret this shift as the Goos-Hänchen shift.

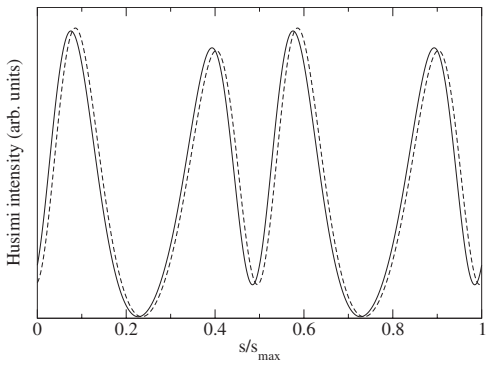

FIG. 8. Incident (solid line) and emerging (dashed line) Husimi function of mode C in Fig. 6 for $p=\sin\chi=0.75$.

In the present section we develop a semiclassical description based on the GHS. We restrict ourselves to systems whose closed counterpart is integrable. Examples are the elliptical and the rectangular cavity. As is well known in the field of quantum chaos, integrable closed systems typically show level crossings rather than avoided level crossings. In the following we consider the crossing point of energy levels where the levels form a pair of degenerate levels. To do so, we use the quantum-mechanical notation for the solutions of the wave equation. We demonstrate that the degeneracy of energy levels implies degenerate ray motion. Degenerate ray motion takes place on resonant tori which are foliated by periodic ray trajectories, in contrast to generic tori which support quasiperiodic motion.

Let us consider two states each labeled by a pair of quantum numbers (n_1,n_2) and (m_1,m_2), respectively. In the limit of large quantum numbers the semiclassical Einstein-Brillouin-Keller (EBK) quantization rule for the actions I_1 and I_2 [45]

$$E_{n_1,n_2} = H\left[\left(n_1+\frac{\alpha_1}{4}\right)\hbar,\left(n_2+\frac{\alpha_2}{4}\right)\hbar\right], \tag{3}$$

$$E_{m_1,m_2} = H\left[\left(m_1+\frac{\beta_1}{4}\right)\hbar,\left(m_2+\frac{\beta_2}{4}\right)\hbar\right] \tag{4}$$

is expected to give accurate results; H is the classical Hamiltonian, and α_i and β_i are Maslov indices [46]. Note that, for systems with separatrices, Maslov indices can be defined only locally in phase space [29,47,48]. However, if both states belong to the same type of classical motion then α_i and β_i are uniquely defined.

Moreover, we assume in the following that $|n_i-m_i| \ll n_i,m_i$. In this regime we can use the Taylor expansion in $\Delta n_i=m_i-n_i$,

$$E_{m_1,m_2} \approx E_{n_1,n_2} + \frac{\partial H}{\partial I_1}\Delta n_1\hbar + \frac{\partial H}{\partial I_2}\Delta n_2\hbar. \tag{5}$$

In the case of degenerate levels $E_{m_1,m_2}=E_{n_1,n_2}$ we can write Eq. (5) with the frequencies $\omega_i=\partial H/\partial I_i$ as

$$\omega_1\Delta n_1 + \omega_2\Delta n_2 = 0. \tag{6}$$

Since Δn_i are integer numbers, Eq. (6) requires that the frequency ratio ω_1/ω_2 is a rational number. As a consequence the corresponding torus is resonant and composed of periodic ray trajectories. This line of arguments shows that the degeneracy of quantum levels is related to the appearance of periodic ray trajectories for the case of integrable closed systems.

When an integrable system is subject to a smooth and generic perturbation then on the quantum (wave) side the degeneracy of the levels is lifted. As a consequence, a level crossing turns into an avoided level crossing. In the case of microcavities the perturbation is given by the open boundary,

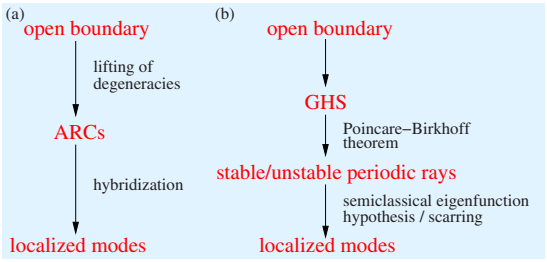

FIG. 9. (Color online) From the open boundary to localized modes near ARCs in systems with integrable closed counterpart. (a) Wave description and (b) semiclassical description with augmented ray dynamics.

which allows for leakage of light out of the cavity. On the classical (ray) side, a generic perturbation breaks up the resonant tori into a chain of stable periodic orbits (ray trajectories) surrounded by islands and unstable periodic orbits surrounded by a chaotic layer. This scenario is proven by the Poincaré-Birkhoff theorem [49,50]. The fate of the nonresonant tori is determined by the Kolmogorov-Arnol'd-Moser (KAM) theorem [51–53]. It states basically that most of the nonresonant tori are conserved in the perturbed system.

The basic idea here is to consider the GHS as a wavelength-dependent perturbation of the ray dynamics. The GHS is a direct consequence of the open boundary. The general scenario is as follows. The GHS creates stable and unstable periodic orbits according to the Poincaré-Birkhoff theorem. The size of the corresponding islands surrounding the stable orbits in phase space depends on the ratio of wavelength to cavity size. We get smaller islands for larger normalized frequencies $\Omega = kR$ and larger islands for smaller Ω. Following the semiclassical eigenfunction hypothesis [54,55], the islands can support modes. In addition, modes can be scarred along the unstable periodic ray trajectories. This semiclassical description is summarized in Fig. 9 together with the wave description. It is important to note that the nonintegrability of the augmented ray dynamics explains the existence of ARCs.

The GHS Δs for a TM polarized plane wave reflected at a planar dielectric interface is according to Artmann [56] given by

$$k\Delta s = \mathrm{Re}\left(\frac{2}{\sqrt{n^2 \sin^2 \chi - 1}} \frac{\sin \chi}{\sqrt{1 - \sin^2 \chi}} \right). \tag{7}$$

The angle of reflection is equal to the angle of incidence χ. Figure 10 shows that the right-hand side of Eq. (7) has singularities at the critical angle $\sin \chi_c = 1/n$ and at $\sin \chi \to 1$. These singularities disappear in the case of incoming waves with finite spatial extension. For Gaussian beams of width σ, Lai *et al.* derived an analytical expression [57]. However, their result is restricted to $k\sigma \gg 1$, and exhibits artificial singularities in the low-$k\sigma$ regime considered here. Therefore, we use the Artmann result (7) for long-lived ray trajectories which stay well within the interval $\sin \chi \in [0.35, 0.9]$. Note that the GHS Δs disappears in the semiclassical (short-wavelength) limit $k \to \infty$. The GHS at curved interfaces has been computed numerically in Refs. [58,59], where, away

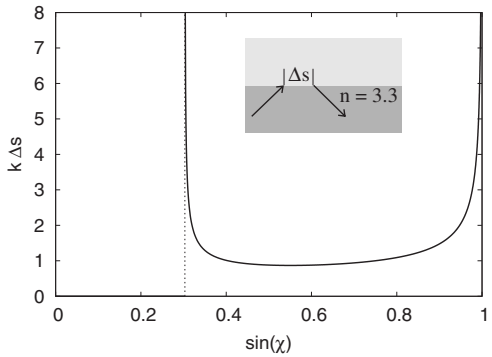

FIG. 10. Goos-Hänchen shift Δs at a planar interface according to Eq. (7). The function Δs is antisymmetric with respect to $\chi \to -\chi$, i.e., the shift measured along the direction of momentum is always non-negative. If $|\sin \chi| < 1/n$ then $\Delta s = 0$. The dashed line marks the critical line $\sin \chi_c = 1/n$.

from the critical angle in the regime of total internal reflection, reasonable agreement with the Artmann result has been found. No analytical formulas are available for the general case.

To compute the augmented ray dynamics, we combine the billiard map $(s_{j+1}, p_{j+1}) = M(s_j, p_j)$ with the Goos-Hänchen map $G(\lambda)$ defined by

$$s_{j+1} = s_j + \Delta s(p_j, \lambda), \tag{8}$$

$$p_{j+1} = p_j. \tag{9}$$

As the map $G(\lambda)$ preserves the phase-space area, the combined map $MG(\lambda)$ is Hamiltonian. In the short-wavelength limit we recover the standard ray dynamics, i.e., $M = \lim_{\lambda \to 0} MG(\lambda)$.

Figure 11 shows the phase-space structure of the augmented ray dynamics for the situation of the rectangular mode at $e \approx 0.649$. The left inset shows that the GHS creates small islands in phase space. The centers of these islands

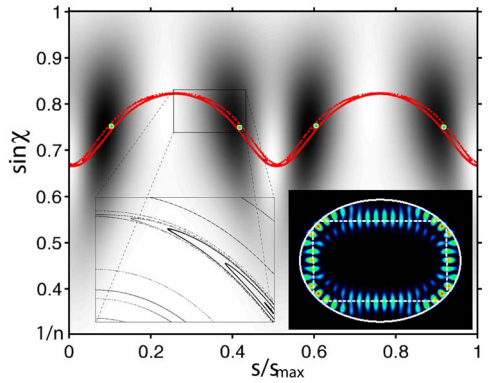

FIG. 11. (Color online) Emerging Husimi function of the rectangular mode (mode C in Figs. 5 and 6) compared to the Poincaré SOS of the augmented ray dynamics above the critical line $\sin \chi_c = 1/n$. The thick dots mark the stable periodic ray trajectory at the center of the islands (dotted curves). Left inset: magnification of one of the islands. Right inset: mode structure and stable periodic ray trajectory in real space. Parameters are as in Figs. 5 and 6.

correspond to stable periodic orbits. The phase space in Fig. 11 has been computed with Eq. (7) for $\Omega=kR=8.2$. It is important to mention that the overall island structure does not depend on Ω; only the size of the islands does. The same island structure is also obtained when the formula of Lai *et al.* is applied for Gaussian beams [57] in the regime of large $k\sigma$ where the formula is valid. From Fig. 11 it can be clearly seen that the Husimi distribution is correlated with the island chain. Note that for both the Husimi distribution and the ray dynamics the outgoing component is shown, i.e., we plot the emerging Husimi distribution [42] and the orbit just after reflection. Figure 11 reveals that the rectangular mode is not a scar with respect to the augmented ray dynamics but a mode existing in a stable island chain following the semiclassical eigenfunction hypothesis. While the center of the Husimi function and the corresponding island agree well, the orientation of the two objects is different. This can be understand by the way the Husimi distribution is constructed. The Husimi distribution can be defined as a Wigner distribution (restricted to the boundary of the cavity) folded with Gaussian wave packets of minimal uncertainty (coherent states) [42]. The relative uncertainty and the orientation of the wave packets can be chosen freely, but usually the orientation is chosen in accordance with the s and p axes of phase space, as is done in Fig. 11. However, one can also choose the orientation in accordance with the orientation of the island under consideration. Such "tilted coherent states" have been used, e.g., in [60]. Moreover, note that the Husimi function for billiards and cavities itself is a semiclassical approximation [42].

The discussed ambiguity of the Husimi distribution is not present for the corresponding wave function in real space shown in the right inset of Fig. 11. In this real-space representation the GHS is directly visible. The real-space plot of the mode and the stable periodic ray trajectory shows much better agreement than in the case of the standard ray dynamics; cf. Fig. 5. In fact the agreement is surprisingly good having in mind that we use the GHS for a planar interface and that $\Omega=8.2$ is deep in the wave regime.

The strong leaking of the Husimi function out of the islands in Fig. 11 can be confirmed by computing semiclassically the number of modes m fitting into an island of size A. From EBK quantization for the action $I=\frac{1}{2\pi}\oint p\, ds=m\hbar$ with $p=n\hbar k \sin\chi$ one gets

$$m=\frac{n\Omega s_{\max}}{2\pi R}A(\Omega), \tag{10}$$

where $A(\Omega)$ is the dimensionless phase-space area spanned by $\sin\chi$ and $s/s_{\max}$; the frequency $\Omega=kR$ is considered as real valued for notational convenience. Numerically we find $A=1.53\times10^{-3}$ and $m=0.04$. The value of m appears to be too small; however, it is well known that small islands can also accommodate modes. This is usually explained by the confinement due to cantori in the phase-space region around the islands [32,61]. In our case the confinement is provided by the KAM tori (the unbroken tori of the elliptical billiard) surrounding the islands visible in the left inset of Fig. 11.

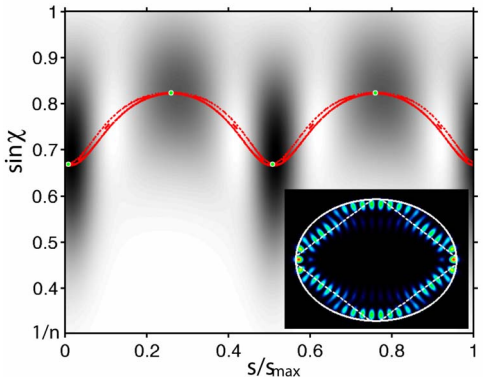

FIG. 12. (Color online) Emerging Husimi function of the diamond mode (mode D in Figs. 5 and 6) compared to the Poincaré SOS of the augmented ray dynamics. The thick dots correspond to the unstable periodic ray trajectory. Inset: mode structure and unstable periodic ray trajectory in real space. Parameters are as in Figs. 5 and 6.

Figure 12 shows the same phase space as before but together with the Husimi function of the diamond mode. Interestingly, this mode is localized on an unstable periodic ray trajectory of the augmented ray dynamics. This periodic ray trajectory is surrounded by a tiny chaotic layer which is not visible in Fig. 12. Hence, the diamond mode is a true scar in the augmented ray dynamics. Again, the real-space plot in the inset shows much better agreement than in the case of the standard ray dynamics; cf. Figure 5

Figure 13 eventually depicts the case of the bowtie mode C with $e\approx0.845$; cf. Figures 2 and 3. Again, the GHS creates islands in phase space. The inset of Fig. 13 shows that the augmented ray dynamics fits the mode structure slightly better than the standard ray dynamics shown in Fig. 2. In the case of Fig. 13 we find for the area $A=4.7\times10^{-3}$ and the number of modes in the islands $m=0.11$. The scenario for the hybridization partner, mode D, results in an unstable periodic ray trajectory (not shown). Here, the GHS affects only the overcritical reflections in the elongated region of the ellipse,

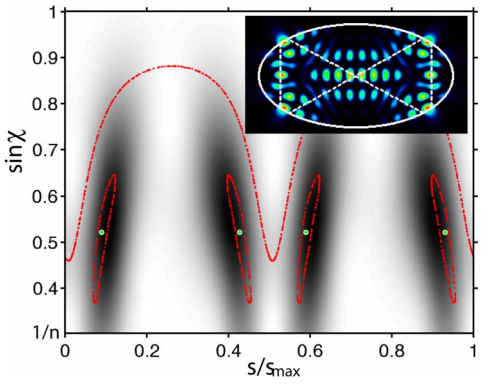

FIG. 13. (Color online) Emerging Husimi function of the bowtie mode (mode C in Figs. 2 and 3) compared to the Poincaré SOS of the augmented ray dynamics. The thick dots mark the stable periodic ray trajectory at the center of the islands. Inset shows the mode structure and the stable periodic ray trajectory in real space. Parameters are as in Figs. 2 and 3.

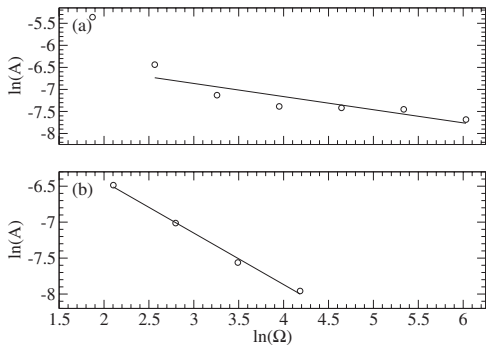

FIG. 14. Size of the island A created by the GHS as function of Ω in log-log plot. (a) Eccentricity $e \approx 0.845$. The line is a linear fit with slope ≈ -0.3. (b) $e \approx 0.649$. The line is a linear fit with slope ≈ -0.72.

whereas the shift is zero at the remaining reflection points because of normal incidence.

Figure 14(a) shows how the size of the islands scales with the frequency Ω in the case of $e \approx 0.845$. For large enough Ω we see a power law dependence with exponent ≈ -0.3. From Eq. (10) it then follows that the number of GHS modes increases as $\Omega^{0.7}$ in the semiclassical limit. Note that the first data point with $\Omega = 8.2$ is not used in the fitting procedure, since the corresponding island is strongly influenced by the critical line; see Fig. 13. For the case $e \approx 0.649$, Fig. 14(b) shows a power law with exponent ≈ -0.72. Here the number of modes in the semiclassical limit scales as $\Omega^{0.28}$. Interestingly, the exponent depends on eccentricity. In both cases the number of GHS-induced modes increases as the semiclassical limit is approached (or the wavelength is fixed and the cavity size is increased).

GHS-induced modes have already been predicted for the case of microdome cavities [62]. However, the relation to ARCs was not revealed in Ref. [62].

V. SUMMARY

We have analyzed the phase-space structure of localized modes formed near avoided resonance crossings. Using the Husimi function we are able to demonstrate the mechanism for the reduction (enhancement) of lifetimes due to constructive (destructive) interference in real space leading to an enhancement (reduction) of intensity in the leaky region of phase space. We have developed a semiclassical extension of the ray model to describe the wave phenomenon of localized modes for systems with integrable closed counterpart. This augmented ray dynamics includes the Goos-Hänchen shift. As the Goos-Hänchen shift breaks the integrability, it naturally explains both the appearance of avoided resonance crossings and the localization of modes. According to the Poincaré-Birkhoff theorem, the perturbation creates stable and unstable periodic ray trajectories along which the modes localize. This scenario shows that half of the scarlike modes of Ref. [15] can be regarded as true scars in the augmented ray dynamics. As example we discussed an optical microcavity with an elliptical cross section, but we expect that our results apply to other cavity geometries as well. Moreover, we believe that the concept of an augmented ray dynamics can also be applied to quantum systems, in particular to soft-wall billiards [32,63], in order to semiclassically describe quantum effects in a conceptually simple way.

ACKNOWLEDGMENTS

We would like to thank A. Bäcker, E. Bogomolny, S. W. Kim, and H. Waalkens for discussions. Financial support by the DFG research group "Scattering Systems with Complex Dynamics" and the DFG Emmy Noether Program is acknowledged.

[1] J. von Neumann and E. P. Wigner, Z. Phys. **30**, 467 (1929).
[2] G. Gamow, Z. Phys. **51**, 204 (1928).
[3] P. L. Kapur and R. Peierls, Proc. R. Soc. London, Ser. A **166**, 277 (1938).
[4] W. D. Heiss, Phys. Rev. E **61**, 929 (2000).
[5] N. J. Kylstra and C. J. Joachain, Phys. Rev. A **57**, 412 (1998).
[6] M. Desouter-Lecomte, J. Liévin, and V. Brems, J. Chem. Phys. **103**, 4524 (1995).
[7] M. Wagner and H. Mizuta, Phys. Rev. B **48**, 14393 (1993).
[8] I. Rotter and A. F. Sadreev, Phys. Rev. E **71**, 036227 (2005).
[9] T. Yoshie, A. Scherer, J. Hendrickson, G. Khitrova, H. M. Gibbs, G. Ruper, C. Ell, O. B. Shchekin, and D. G. Deppe, Nature (London) **432**, 200 (2004).
[10] J. Reithmaier, G. Sek, A. Löffler, C. Hofmann, S. Kuhn, S. Reitzenstein, L. Keldysh, V. Kulakovskii, T. Reinecke, and A. Forchel, Nature (London) **432**, 197 (2004).
[11] E. Peter, P. Senellart, D. Martrou, A. Lemaitre, J. Hours, J. M. Gérard, and J. Bloch, Phys. Rev. Lett. **95**, 067401 (2005).
[12] E. Persson, I. Rotter, H.-J. Stöckmann, and M. Barth, Phys. Rev. Lett. **85**, 2478 (2000).
[13] C. Dembowski, H.-D. Gräf, H. L. Harney, A. Heine, W. D. Heiss, H. Rehfeld, and A. Richter, Phys. Rev. Lett. **86**, 787 (2001).
[14] J. Wiersig and M. Hentschel, Phys. Rev. A **73**, 031802(R) (2006).
[15] J. Wiersig, Phys. Rev. Lett. **97**, 253901 (2006).
[16] M. Desouter-Lecomte and V. Jacquest, J. Phys. B **28**, 3225 (1995).
[17] E. J. Heller, Phys. Rev. Lett. **53**, 1515 (1984).
[18] F. J. Arranz, F. Borondo, and R. M. Benito, Phys. Rev. Lett. **80**, 944 (1998).
[19] F. Goos and H. Hänchen, Ann. Phys. (Leipzig) **436**, 333 (1947).
[20] K. J. Vahala, Nature (London) **424**, 839 (2003).
[21] J. U. Nöckel and A. D. Stone, Nature (London) **385**, 45 (1997).
[22] C. Gmachl, F. Capasso, E. E. Narimanov, J. U. Nöckel, A. D. Stone, J. Faist, D. L. Sivco, and A. Y. Cho, Science **280**, 1556

(1998).
[23] H. G. L. Schwefel, N. B. Rex, H. E. Tureci, R. K. Chang, and A. D. Stone, J. Opt. Soc. Am. B **21**, 923 (2004).
[24] S. Sunada, T. Harayama, and K. S. Ikeda, Opt. Lett. **29**, 718 (2004).
[25] S. A. Backers, A. P. Heberle, J. R. A. Cleaver, and K. Köler, Phys. Status Solidi B **204**, 581 (1997).
[26] S.-K. Kim, S.-H. Kim, G.-H. Kim, H.-G. Park, D.-J. Shin, and Y.-H. Lee, Appl. Phys. Lett. **84**, 861 (2004).
[27] J. D. Jackson, *Classical Electrodynamics* (John Wiley and Sons, New York, 1962).
[28] J. Wiersig, J. Opt. A: Pure Appl. Opt. **5**, 53 (2003).
[29] H. Waalkens, J. Wiersig, and H. R. Dullin, Ann. Phys. (N.Y.) **260**, 50 (1997).
[30] H. Waalkens, J. Wiersig, and H. R. Dullin, Ann. Phys. (N.Y.) **276**, 64 (1999).
[31] H.-J. Stöckmann, *Quantum Chaos* (Cambridge University Press, Cambridge, U.K., 2000).
[32] B. Weingartner, S. Rotter, and J. Burgdörfer, Phys. Rev. B **72**, 115342 (2005).
[33] R. Hofferbert, H. Alt, C. Dembowski, H.-D. Gräf, H. L. Harney, A. Heine, H. Rehfeld, and A. Richter, Phys. Rev. E **71**, 046201 (2005).
[34] R. G. Scott, S. Bujkiewicz, T. M. Fromhold, P. B. Wilkinson, and F. W. Sheard, Phys. Rev. A **66**, 023407 (2002).
[35] P. B. Wilkinson, T. M. Fromhold, L. Eaves, F. W. Sheard, N. Miura, and T. Takamasu, Nature (London) **380**, 608 (1996).
[36] A. Kormányos, Z. Kaufmann, J. Cserti, and C. J. Lambert, Phys. Rev. Lett. **96**, 237002 (2006).
[37] J. Wiersig and M. Hentschel, Phys. Rev. Lett. **100**, 033901 (2008).
[38] S. B. Lee, J. H. Lee, J. S. Chang, H. J. Moon, S. W. Kim, and K. An, Phys. Rev. Lett. **88**, 033903 (2002).
[39] W. Fang, A. Yamilov, and H. Cao, Phys. Rev. A **72**, 023815 (2005).
[40] T. Fukushima, T. Harayama, and J. Wiersig, Phys. Rev. A **73**, 023816 (2006).
[41] N. B. Rex, H. E. Tureci, H. G. L. Schwefel, R. K. Chang, and A. D. Stone, Phys. Rev. Lett. **88**, 094102 (2002).
[42] M. Hentschel, H. Schomerus, and R. Schubert, Europhys. Lett. **62**, 636 (2003).
[43] S.-Y. Lee, J.-W. Ryu, T.-Y. Kwon, S. Rim, and C.-M. Kim, Phys. Rev. A **72**, 061801(R) (2005).
[44] E. G. Altmann, G. Del Magno, and M. Hentschel (unpublished).
[45] J. B. Keller, Ann. Phys. (N.Y.) **4**, 180 (1958).
[46] V. P. Maslov, *Théorie des Perturbations et Méthodes Asymptotiques* (Dunod, Paris, 1972).
[47] P. H. Richter, H. R. Dullin, H. Waalkens, and J. Wiersig, J. Phys. Chem. **100**, 19124 (1996).
[48] J. Wiersig, Z. Naturforsch., A: Phys. Sci. **57**, 537 (2001).
[49] E. Ott, *Chaos in Dynamical Systems* (Cambridge University Press, Cambridge, U.K., 1993).
[50] A. J. Lichtenberg and M. A. Lieberman, *Regular and Chaotic Dynamics* (Springer, Berlin, 1992).
[51] A. N. Kolmogorov, Dokl. Akad. Nauk SSSR **98**, 527 (1954).
[52] V. I. Arnol'd, Russ. Math. Surv. **18**, 85 (1963).
[53] J. Moser, Nachr. Akad. Wiss. Goett. I, Math.-Phys. Kl. **2**, 1 (1962).
[54] I. C. Percival, J. Phys. B **6**, L229 (1973).
[55] M. V. Berry, J. Phys. A **10**, 2083 (1977).
[56] K. Artmann, Ann. Phys. (Leipzig) **8**, 270 (1951).
[57] H. M. Lai, F. C. Cheng, and W. K. Tang, J. Opt. Soc. Am. A **3**, 550 (1986).
[58] M. Hentschel and H. Schomerus, Phys. Rev. E **65**, 045603(R) (2002).
[59] H. Schomerus and M. Hentschel, Phys. Rev. Lett. **96**, 243903 (2006).
[60] A. Bäcker, R. Ketzmerick, and A. G. Monastra, Phys. Rev. Lett. **94**, 054102 (2005).
[61] J.-B. Shim, S.-B. Lee, S. W. Kim, S.-Y. Lee, J. Yang, S. Moon, J.-H. Lee, and K. An (unpublished).
[62] D. H. Foster, A. K. Cook, and J. U. Nöckel, Opt. Lett. **32**, 1764 (2007).
[63] A. Kaplan, N. Friedman, M. Andersen, and N. Davidson, Phys. Rev. Lett. **87**, 274101 (2001).